

# Optimization of a Radiofrequency Ablation FEM Application Using Parallel Sparse Solvers

Marcelo Cogo Miletto\*, Claudio Schepke<sup>†</sup>, Lucas Mello Schnorr\*

\* Institute of Informatics, Federal University of Rio Grande do Sul, Porto Alegre, Brazil

<sup>†</sup> UNIPAMPA, Alegrete, Brazil

**Abstract**—Finite element method applications are a common approach to simulate a handful of phenomena but can take a lot of computing power, causing elevated waiting time to produce precise results. The radiofrequency ablation finite element method is an application to simulate the medical procedure of radiofrequency ablation, a minimally invasive liver cancer treatment. The application runs sequentially and can take up to 20 hours of execution to generate 15 minutes of simulation results. Most of this time arises from the need to solve a sparse system of linear equations. In this work, we accelerate this application by using three sparse solvers packages (MAGMA cuSOLVER, and QRMumps), including direct and iterative methods over different multicore and GPU architectures. We conducted a numerical result analysis to access the solution quality provided by the distinct solvers and their configurations, proposing the use of the peak signal-to-noise ratio metric. We were able to reduce the application execution time up to 40 times compared to the original sequential version while keeping a similar numerical quality for the results.

## I. INTRODUCTION

Scientific computing is a powerful domain to impel progress in many fields of research. However, it is one of the most computing power demanding activities, requiring a significant amount of computing time to produce precise results in a feasible time. Many classical ideas, such as the Finite Element Method (FEM), gained popularity through the computational power support provided by modern hardware, enabling scientists to deal with huge problems. FEM is nowadays widely used in the industry and academy to simulate numerous phenomena. It is described as a unified approach to various problems, and universally adaptable to discrete systems [1].

Such a standard computational method to tackle a handful of problems is also widely studied. There are common steps in a FEM application that are particularly interesting to look at when we are concerned about the application performance. First, the global matrix assembly step groups all element equations to represent the whole problem. Then, obtaining the solution to this system of linear equations represents the two most time-consuming steps. Furthermore, the global matrix generally is very sparse since FEM is used to approximating partial differential equations (PDEs), and PDEs are a common source of sparse matrices [2]. Therefore, such applications cannot use basic factorization algorithms since the fill-in overhead would be catastrophic for performance. Hence, such problems demand the use of efficient sparse matrix solvers.

The performance of sparse solvers, as well as for dense solvers, is obtained through parallelizing the solution process.

Numerous libraries use different methods and approaches, exploring parallelism in several computational resources using different programming paradigms. Libraries such MAGMA [3] and CUSOLVER [4], focus on providing a broad set of smaller routines in a BLAS-like way, and complete solvers for both dense and sparse matrices, containing direct and iterative solvers. On the other hand, solvers like QRMumps [5], and PASTIX [6], focus on providing a unique, specialized sparse direct solver for general sparse matrix and symmetric matrix.

The Radiofrequency Ablation FEM (RAFEM) [7] simulates the Radiofrequency Ablation (RFA) procedure using the FEM. Its original code runs sequentially, making the simulation method very slow because of the computing-intensive steps involved in FEM simulations. Furthermore, it uses the Frontal Method [8] for the solve step, which is a solution for memory-efficiency but not for performance. Given these application characteristics, the waiting time for simulating results can be excessive, taking up to 20 hours to simulate 15 minutes of the RFA procedure. Our work focus on the parallelization, numerical analysis, and performance evaluation of the RAFEM application. We explore the capacity of GPGPUs and multicore systems to parallelize and accelerate the application, focusing on the solve steps, using multiple modern libraries to obtain the equation system solution. The contributions are as follows:

- We implemented a parallel version of the RAFEM application that works with multiple sparse solvers.
- Tested and adapted the Fortran C interface of the QRMumps application to a real application scenario.
- We describe the parallelization methodology of the application using GPU, and the role of sparse solvers, which can be valuable for other FEM applications [9], [10], including other RFA simulation software.
- Conducted experiments in different machines with multiple solvers to analyze the performance considering two workloads in the RAFEM application context. We evaluate numerical results for each solver used, comparing it to the original sequential version results.

The paper is organized as follows: Section II describes the background concepts for this work, Section III describe the methodological aspects and materials. The Section IV present the analysis of the numerical results, followed by Section V that presents the application performance analysis. Lastly, Section VI presents the conclusion, recapping the interesting points, and discussing future work.

## II. BACKGROUND

We describe the RAFEM application and its main loop in Figure 1, pinpointing the application execution flow, its two most costly parts and the role of parallel sparse solvers.

### A. The RAFEM application

RFA is a minimally invasive medical procedure. The RAFEM application simulates the RFA for treating hepatic cancer. The procedure consists of using the Joule heating energy from a special electrode connected to an alternated current generator to eliminate cancer cells by heating the desired liver region. After the positioning of the electrodes inside the patient's liver, when the RFA starts, techniques like computed tomography or magnetic resonance imaging are unable to provide precise observations to inspect the temperature distribution area during the actual procedure [7].

To the procedure be successful, the heated area in the liver must eliminate all cancer cells. Otherwise, tumor recidivism can occur. To understand and adjust the procedure parameters for each treatment case, specialists must know, beforehand, the total heated area in the liver. Thus, simulation can increase the chances of success of the procedure in avoiding resubmitting the patient to a new RFA procedure. The RAFEM application development was to help clinician specialists find the best parameters for each treatment case through computer simulation. The application uses the FEM to simulate the heat and voltage distribution along time in a mesh of tetrahedral elements.

**Main application loop:** The application uses the predictor-corrector method to extrapolate the solution further in time, then correct it until reaching a convergence threshold value. The Figure 1 depicts the principal application execution flow. After the pre-processing part of reading data and setting initial values for the problem, it enters a loop that controls the total simulated time, advancing in dynamically sized time steps of size  $\Delta t$  [7]. The loop performs  $n$  steps, which depends on the total simulation time. For each one of these steps, it executes the corrector step until the desired convergence threshold is satisfied. For this corrector step, the application computes all the element equations with updated values and assembly them in the global matrix that is structurally symmetric and sparse, which needs to be solved by a sparse matrix solver. This corrector step is the most costly in the application. It runs many times and contains the two most time-consuming phases of FEM applications: the global matrix assembly and solve.

**Assembly step:** Many advances focus on these steps towards exploring the use of GPUs to accelerate them [11]. For the assembly step, including numerical integration, a variety of works study different approaches, focusing on accelerating this step using GPUs. Approaches consider using better formats to represent and assembly the global matrix besides the most common ones, like the proposed adapted coordinate (COO) and the ELLpack (ELL) format [12], [13]. Furthermore, designing specialized algorithms and data structures aligned to GPU programming specific concepts like dynamic GPU memory allocation, thread-block shared memory, and warps [12], [14] seems to be a common approach. The authors

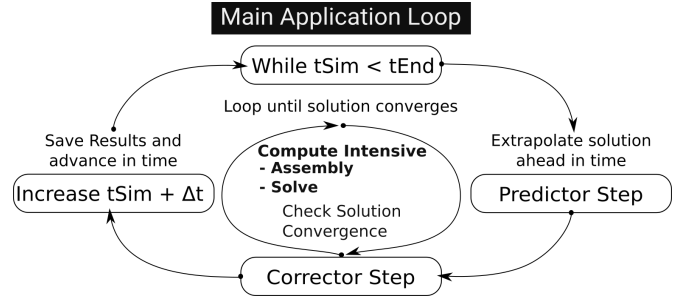


Fig. 1. Main loop of the RAFEM application.

discuss the advantages and disadvantages of using techniques like graph coloring, graph partitioning, atomic operations, and precomputed structures to handle race conditions. For which there is not a consensus on what is the best strategy. The best approach depends on the problem structure and mesh type, computational capability of the devices, and the FEM parallelization approach. For example, despite those works that use GPU to accelerate the global matrix assembly in a sparse matrix format, some GPU FEM problems are modeled in the Element-by-Element FEM (EbE-FEM) approach [15], [16], which avoids explicitly assembling the global matrix to obtain its solution.

**Solve Step:** For the solve phase, the advances are essentially expressed by the wide variety of parallel iterative and direct sparse solvers that we have available today. The solvers use different approaches, like in the GPU-specific libraries that have collections of parallel solvers that fit in many cases [4], [3]. Besides these libraries and their comprehensive set of routines, other approaches focus on developing specialized tuned algorithms. These specialized algorithms are often used for sparse direct solvers because they are more challenging in the aspects of parallelization, communication, and scalability. The MUMPS [17] solver is one of the earliest distributed memory parallel sparse solvers, capable of distributing and balancing the work among many cores. MUMPS achieved such capability through the dynamic scheduling of computational tasks, manually implemented and extracted from the algorithm's knowledge. Nowadays, many high-performance direct sparse solvers follow a task-based approach, looking to achieve performance scalability and ease in managing the tasks. Solvers like QRMumps [5], and Pastix [6] are examples of solvers that rely on a task-based approach, allowing them to use powerful scheduling algorithms and the possibility to explore heterogeneous computational resources. There are also parallel GPU solvers designed especially for EbE-FEM problems [18].

### B. Parallel Sparse Solvers

Consider the problem of solving a linear system of equations in the form of  $Ax = b$ . Essentially, there are two families of solvers [19]: the direct solvers and the iterative solvers. These two kinds of methods fit for solving both sparse and dense systems of linear equations. The major difference between

these approaches is that direct methods use a finite number of elemental operations to factorize the input matrix  $A$  into a form that obtaining the solution becomes trivial. Iterative solvers obtain the solution by performing a sequence of approximations of the solution using matrix-vector multiplications. The cost of such methods can be said to be  $IN^2$ , where  $I$  is the number of necessary iterations to obtain a solution that is sufficiently close to the real solution given a tolerance value. While iterative methods naturally fit for sparse problems because they do not change matrix structure, direct solvers must use specialized algorithms and data structures to obtain advantage from the matrix sparsity.

Some methods utilization depends on the particular matrix properties. Thus, the type of solver and which algorithm to use is dependent on the type of problem matrix. For symmetric positive-definite matrices, for example, the direct method of Cholesky factorization and the Conjugate Gradient iterative method are very common choices. However, when the matrix properties do not hold, we must use other methods like the Restarted Generalized Minimal Residual Method GMRES(m) and the sparse QR factorization. The cost of direct methods for sparse factorization depends much on the specific algorithm implemented and the matrix sparsity pattern. These factors have a significant influence on the total fill-in introduced during factorization. For this, sparse factorization is commonly preceded by an analysis step. This analysis step is responsible for applying fill-reducing permutations in the original matrix such as the Reverse Cuthill-McKee, Average Minimum Degree, and Nested Dissection reorderings. The permutation is commonly followed by a symbolic factorization step to compute the final matrix structure. Analogous to this analysis step in direct sparse factorization. Iterative solvers may suffer from a low convergence rate when we have big sparse problems or ill-conditioned matrices. Preconditioners are applied to alleviate this effect, accelerating the solver convergence rate.

### III. METHODS AND MATERIALS

We present the methodological workflow of this paper, as depicted in Figure 2. The workflow starts with the data collection, involving the parallelization and instrumentation, and the execution of our experiments. Then, executions can generate two types of results: the ScoreP OTF2 trace results and the simulated results written to a binary file. These raw files need to be post-processed in the conversion step, enabling us to work with the data files to derive metrics and create visual representations for numerical and performance analysis.

#### A. Parallelizing Application

The assembly stage parallelization was done in a previous work [20] by implementing CUDA kernels that were responsible for assembling the individual elements equations and grouping them in the Compressed Sparse Row (CSR) sparse matrix format to represent the global matrix. Despite all the promising techniques for the assembly phase presented in Section II, we kept this simpler approach of assembling

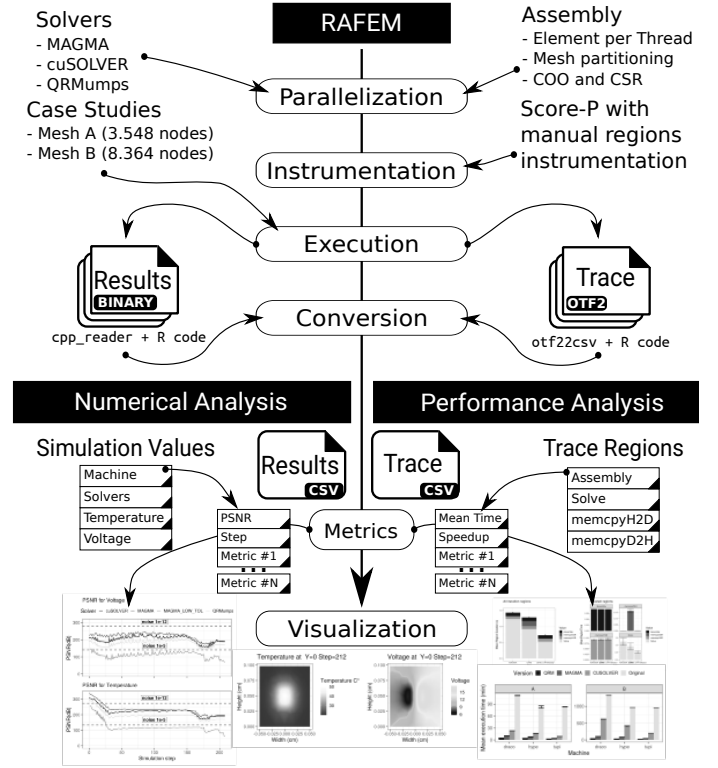


Fig. 2. Methodological workflow overview from application parallelization and instrumentation, to data collection and visual presentation.

the element matrices individually (one thread by element) and assigning them in the global matrix by mapping threads to assembly specific matrix regions, similar to a graph partitioning approach to avoid race conditions. Thus, there is a potential improvement to explore in the assembly part. However, we focus on the solve phase in the RAFEM application as the most significant computational part arises from it.

The previous work already used MAGMA for the solution phase but did not explore different solvers and computational environments. Besides the MAGMA solution, we analyze two more solvers in this work: the sparse QR factorization from cuSOLVER, done entirely in GPU, and the task-based QR sparse factorization from QRMumps, using CPUs. The previous code assembly the matrix in the CSR format, which fits for MAGMA and cuSPARSE solver methods. However, QRMumps expects a matrix in the COO format as input. Thus we extended the CUDA kernel that does the matrix assembly in CSR format to create the COO rows representation array for the QRMumps solver. We employ the QRMumps C-Fortran interface to include the solver in the application.

For the QRMumps solver, in every corrector step iteration (innermost loop in Figure 1), we make an extra memory copy of the global matrix sparse representation from the GPU to the CPU. Moreover, a copy of the solution needs to be in the GPU for the next assembly step. These copies are unnecessary for the GPU solvers since the solution is already in the GPU. However, we need to copy the solution back to CPU every

corrector iteration for the GPU solution phase. This last copy is needed because the application performs the predictor step, the convergence check of the corrector step, and the time increment calculation sequentially as the original code do. Nonetheless, the total execution time impact difference implied by these extra copies is neglectable (below 0,15%). Lastly, we parallelize seven out of eleven vector reduction operations and transformations that arise from the prediction, assembly, and solve steps using the `thrust` library and its operations `transform` and `transform_reduce`.

### B. Solver Tuning

Having the three solvers working, we started to study parameters that affect their performance. The matrix reordering algorithm is crucial for direct solvers to enhance parallelism and control the fill-in effect. For `QRMumps`, we explored the Scotch [21] and Metis [22] reordering algorithms. Metis provided better acceleration for the matrix factorization, which was the best reordering for `cuSOLVER` QR as well. Regarding the `QRMumps` application, as it performs a tiled Householder QR factorization, we need to set the dimensions of the blocks and internal blocks. We have chosen the values of 320 and 32, respectively, which are typical values for this type of configuration. Furthermore, We compiled `QRMumps` with the StarPU 1.3.3 [23], a task-based library that handles the tasks creations and distribution among computational resources. We configured the solver scheduler to use the local-work stealing (LWS) strategy, which presents good performance for CPU-only environments [24].

Studying the problem, we noticed that the matrix structure remains the same, which allows us to reuse the column permutation done in a previous step. By reusing the reordering, we save time in the analysis phase that precedes the factorization. Unfortunately, the `cuSOLVER` function call does not enable passing a user-defined reordering as `QRMumps` do. To contribute to the flexibility of the solver, we made a patch for `QRMumps` C-Fortran interface. This patch enables the user to retrieve the array containing the column reordering made by the chosen reordering algorithm. With access to this array, we can reuse it in later iterations of the solve phase for the `QRMumps` application.

Lastly, the `MAGMA` library method `GMRES(m)` has the parameter  $m$  that impacts the solver convergence rate, which directly affects its performance by increasing or decreasing the number of needed iterations to reach the desired tolerance for the residual value. Recognizing this effect, we did some previous experiments to find a fair value of  $m$  for our tested workloads, as presented in Figure 3. In the left part of the figure, we have the  $m$  values in the x-axis, and how many times the total application execution time was slower than the smaller execution time obtained for that value of  $m$ . We could achieve further improvements in the `MAGMA` `GMRES(m)` method efficiency if it incorporates some ideas, such as using an adaptative  $m$  value during the simulation and for each solution [25]. Such improvements can reduce stagnation effects observed in the right part of the Figure 3, which occurs

even for the best-picked values for some iterations of the solve phase. Moreover, we set the convergence tolerance for the `GMRES(m)` method to  $10^{-10}$  in our experiments.

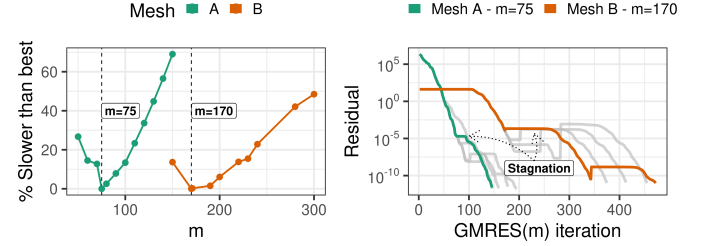


Fig. 3. Best value for  $m$  in each mesh (left), and stagnation effect (right).

### C. Tracing Code Regions

A common approach to improving application performance is first understanding the application behavior to identify possible performance bottlenecks and improvement points. A popular way to do it is by application tracing and profiling. The ScoreP [26] library provides a simple user-defined tracing, allowing the user to manually define tracing of code regions areas that the user judges interesting. These regions tracing help collect simple measurements in application-specific points without generating too much overhead in application execution time caused by tracing intrusion [26].

We focused on tracing the costly computing regions of the corrector step, including the assembly and solve parts and all the data movements between CPU and GPU. This tracing enables us to characterize the computational cost of this part of the application in four different common regions: Assembly, Solve, `memcpyH2D` (memory copies from the host (CPU) to the device (GPU)), and `memcpyD2H` (from device to host). Thus, we have a detailed view of the application performance, which can help in the decision of optimizing one of these parts and predicting how much we can reduce the total execution time by its optimization. The ScoreP tool records application trace in the OTF2 format. We used a conversion tool named `otf22csv`<sup>1</sup> to transform the OTF2 trace data into the CSV format, enabling the analysis with modern data analysis tools like the R language.

### D. Experimental Context and Workload Detail

We used machines with different hardware capabilities to evaluate the performance of the studied solvers. The machines description is listed in Table I. All of them used CUDA version 10.2.89, `MAGMA` version 2.5.2, and StarPU 1.3.3 and openblas 0.3.9 for `QRMumps`. The major difference between them is the number of CPU cores and the GPU specifications. Table II presents the two different resolutions of finite element meshes that describe the liver and the electrodes used as workloads. Both meshes A and B produce square and very sparse matrices. To obtain metrics to calculate mean execution time and speedup, we used a full factorial design considering the three

<sup>1</sup><https://github.com/schnorr/otf2utils>

factors machine(3), workload(2), and solver(4). Making 30 repetitions for the smaller workload A and 10 for the bigger one B. In total, we performed 480 executions to obtain the performance metrics.

TABLE I  
HARDWARE INFORMATION OF MACHINES USED IN THE EXPERIMENTS.

Machine	CPU	GPU	CUDA cores
Draco	2x8 E5-2640v2 - 2.0 GHz	Tesla K20	2,496 - 706 MHz
Hype	2x10 E5-2650v3 - 2.3 GHz	Tesla K80	4,992 - 824 MHz
Tupi	1x8 E5-2620v4 - 2.1 GHz	GTX 1080Ti	3,584 - 1,582 MHz

TABLE II  
WORKLOAD INFORMATION USED IN THE EXPERIMENTS.

Mesh	# Nodes	# Elements	Matrix size	Nonzeroes	Sparsity
A	3,548	18,363	7,096x7,096	189,462	0.0037%
B	8,364	44,811	16,728x16,728	450,451	0.0016%

#### IV. NUMERICAL RESULTS VALIDATION

Most important than accelerating the application, is to check if the parallel versions still producing valid numerical results. As there is no such thing as infinite precision in floating-point numbers, we are limited to the machine epsilon or machine precision. This precision limit can cause roundoff errors that can be magnified or propagated during the application execution. Another aspect that needs attention when evaluating precision is that we are running operations in parallel so that the rounding order may produce slightly different results. Lastly, operations like the Fused Multiply-Add (FMA), present in NVIDIA GPUs, perform operations of type  $XY + Z$  using a single rounding step. Because of this, the computation of the results is more accurate [27].

To evaluate and quantify the quality of our numerical solution obtained by the multiple solvers used, we propose using the Peak Signal-To-Noise Ratio (PSNR) [28], a common metric used for quality estimation involving images. We compare the binary written values for the temperature and voltage along simulation steps produced by RAFEM. We used the original sequential version results as the values that remain unaffected by noise. Then, we compare each step solution using the following formula for calculating PSNR:

$$PSNR_i = 20 \times \log_{10} \times \frac{MAX(A)}{\sqrt{MSE_i}}, \quad (1)$$

where the Mean Squared Error (MSE) is

$$MSE_i = \frac{1}{n} \times \sum_{j=1}^n [A_{ij} - B_{ij}]^2 \quad (2)$$

The  $PSNR_i$  value represents the PSNR value for simulation step  $i$ ,  $MAX(A)$  is the maximum observed value for temperature or voltage among all steps,  $n$  is the number of nodes of the mesh, and  $A_i$  and  $B_i$  are the original and some parallel version solution for all nodes  $j$  in step  $i$ . Accordingly, we defined a PSNR value for each of the simulation

steps to generate the Figures 4 and 5. In these figures, we included different configurations for MAGMA and cuSOLVER to observe their impact on this metric. The `MAGMA_low_tol` is the MAGMA GMRES( $m$ ) solver with a tolerance of  $10^{-6}$  compared to the MAGMA that uses a tolerance of  $10^{-10}$ . The `cuSOLVER_fmadvff` is the cuSOLVER version compiled with the flag `--fmadvff=false`, which disables the GPU's FMA operation. Lastly, the red dashed lines present control values to know what PSNR value we have when calculating it using the original solution values summed with a noise of  $10^{-5}$  and  $10^{-12}$  in each mesh node.

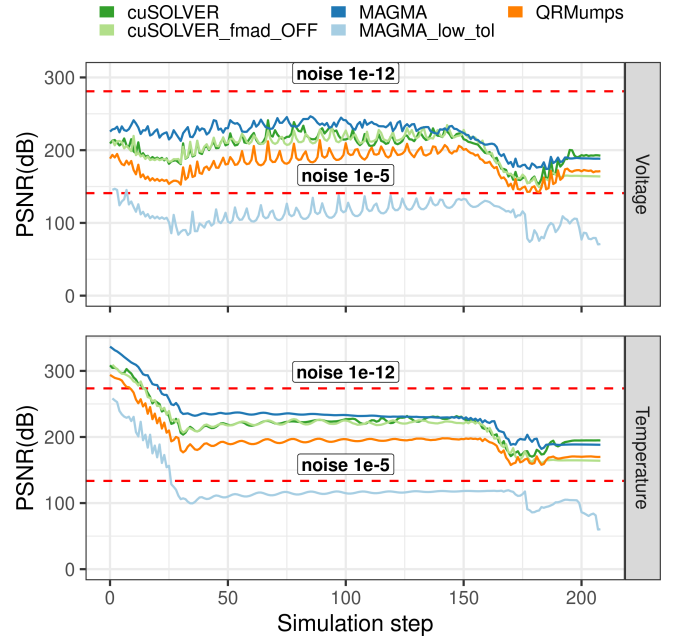


Fig. 4. PSNR for voltage and temperature for mesh A.

We observe that despite the `MAGMA_low_tol` PSNR value for mesh A (Figure 4), the QRMumps solver presented a lower value for PSNR, indicating higher differences in the numerical results. In contrast, cuSOLVER, which also performs the QR sparse factorization, presented a higher value for PSNR. Even when FMA disabled (`cuSOLVER_fmadvff`), except in the last steps for mesh A (Figure 4). The other interesting result that we observe is how the FMA operation changes the PSNR values a bit for cuSOLVER, mainly in the B mesh (Figure 5).

For the `MAGMA_low_tol`, we can observe in Figure 4 that it presents a much lower PSNR value than the others. We also noticed in this case that the corrector step did not converge in less than the maximum allowed iterations (50) for step number 208. When this occurs, the RAFEM application does not accept the solution for that step and reduces the time step size in half. So there is a mismatch in time after that, but the last step represents the same final time, which is the total simulated time, set to 15 minutes for all experiments. However, for the bigger case B in Figure 5, the `MAGMA_low_tol` presented a higher PSNR than other solvers, being just below the MAGMA solution with a tolerance of  $10^{-10}$ . In the overall view, this metric shows us that different solvers and configurations



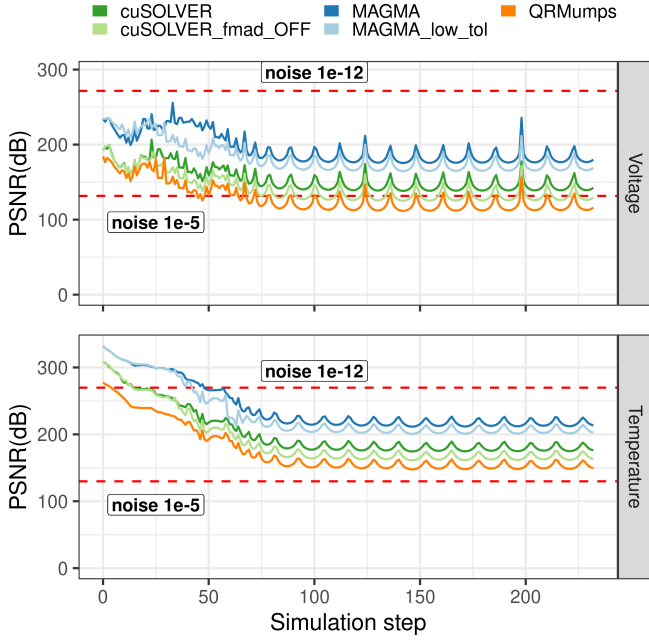


Fig. 5. PSNR for voltage and temperature for mesh B.

provide slightly different numerical results. However, their increase and decrease behavior for the PSNR value is very similar, except for the case where the solution correction at step 208 does not converged for mesh A.

One drawback of using the PSNR metric is that it summarizes the distribution of the numerical differences, hiding them in this metric. For example, PSNR is incapable of telling us if there are many small differences or fewer more significant differences for the simulated values at a given step. Furthermore, we are also unable to observe the spatial dispersion of these differences. Hence, we used the binary file results to generate 2D surface plots of the step that presented lower PSNR value (step 177 for mesh A), presenting the difference of the values from the original solution in a spatial way. We fixed the Y value as 0, which cuts the two electrodes of the mesh in the middle, providing a view of them side-by-side. Figure 6 presents the original values for temperature and voltage at step 177 for the same case execution of Figure 4. We observe that the temperature spread is symmetrical as well as the voltage, but with lower values in one side to create the current flow between the electrodes. We used the *akima* [29] R package to create the 2D interpolation of the values.

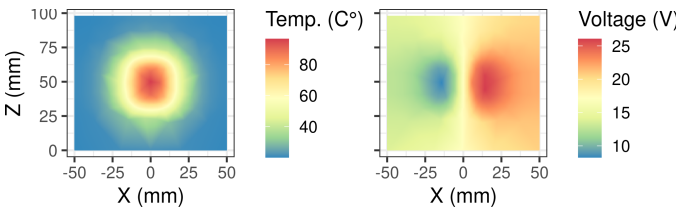


Fig. 6. Original results for step 177 with the electrodes side-by-side. Distribution of temperature (left), and voltage (right).

The Figure 7 presents the visualization of the absolute differences, showing the temperature on the left side, the voltage on the right, and facetting plots by the solvers. Note that the difference in color scale and value magnitude is very different between temperature and voltage. In general, we observe that the area between X  $[-25, 25]$  and Z  $[25, 75]$  holds most of the numerical differences, which is the area near the position of the electrodes. These figures enable us to see that no significant numerical differences have arisen in a spatial sense, spreading only around that area and did not appear in the edges, for example.

We note that, as the PSNR value indicated, the MAGMA solution is much closer to the original than the others, for both temperature and voltage. The differences increase from cuSOLVER to QRMumps, but all solvers present the differences around the same area. The maximum absolute difference values are still low, for example,  $4e-6$  in the QRMumps voltage. However, for the MAGMA\_low\_tol case, in Figure 8 we have a much bigger scale, and the area where the numerical differences appear seems to be wider than the others. For this configuration of the GMRES( $m$ ) solver, we could perhaps start noticing visual differences in the final results presentation, which may invalidate the simulation procedure.

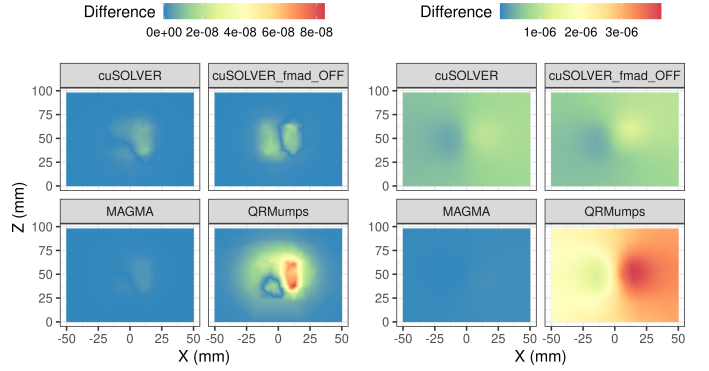


Fig. 7. Numerical differences of step 177 for temperature (left) and for voltage (right), facing the electrodes side-by-side ( $Y = 0$ ).

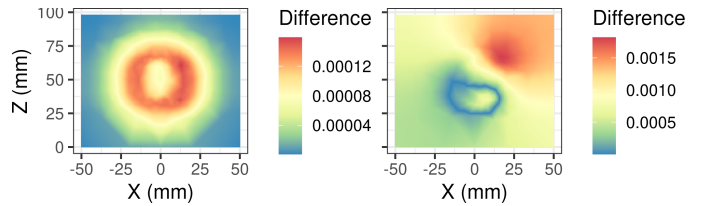


Fig. 8. Numerical differences of MAGMA with lower tolerance for temperature (left) and for voltage (right).

## V. PERFORMANCE EVALUATION

We conducted experiments with different machines and solvers, collecting the total application execution time. Figure 9 presents the overview of the execution time by machine and solver, considering a confidence level of 99.7% after checking that the collected data is normality distributed. We

can observe that the QRMumps solver was faster than the others for all machines and workloads, but the time difference between the GPU solvers and QRMumps is reduced when we have a more powerful GPU in the Tupi machine. We also notice that the sequential version is significantly faster for the Hype and Tupi machines than in Draco, due to the faster CPUs.

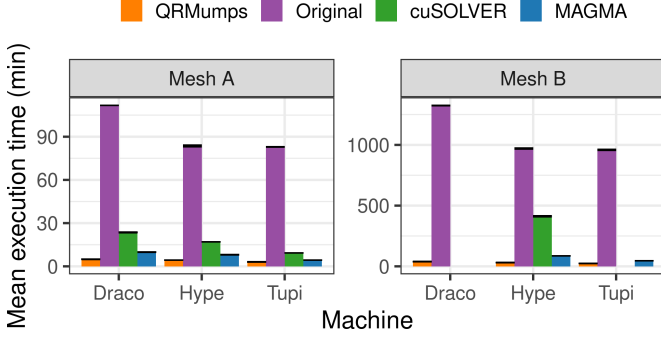


Fig. 9. Makespan for the different machines and solvers.

We present the speedup metric in Figure 10, where we can better observe the effect of more powerful GPUs in the application acceleration, principally among the GPU solvers. However, when we focus on the different workloads, we observe a lower speedup for cuSOLVER for the bigger input mesh B. This cuSOLVER results for the mesh B suggest that its QR solver does scale well for bigger problems. MAGMA and QRMumps presented a higher speedup for mesh B, but the MAGMA increase was around one or two times faster.

In contrast, QRMumps presented increases around 13 times in the speedup for mesh B, reaching up to 40 times of speedup compared to the sequential version in the Tupi machine. However, for the QRMumps solver, we noticed that although the original sequential version makespan is very similar for Hype (966 min) and Tupi (956 min), the speedup in the Tupi machine is higher than in the Hype machine, which has more than twice the number of CPU cores than Tupi. This difference may suggest that there is not enough parallelism in the matrix factorization. Probable causes of this lack of parallelism might come from the matrix structure itself and the configuration parameters used in the QRMumps solvers. Thus, further optimizations can explore better parameter values for these specific cases.

A part of this speedup comes from the assembly step, where better GPUs will run faster because it is a well scalable problem. We can observe in Figure 11 the differences in the mean duration of the traced regions between all step iterations. This figure also included the version MAGMA\_low\_tol to represent how lowering the tolerance in the solve step for the GMRES( $m$ ) iterative solver affects its duration. Nonetheless, we report that lowering the tolerance to  $10^{-6}$  can reduce the total computation time by up to 20%. However, the reduction was less significant for some cases because the application needed to execute more correction steps to reach the desired convergence threshold value. Moreover, the tolerance reduction may cause terrible effects in the numerical results,

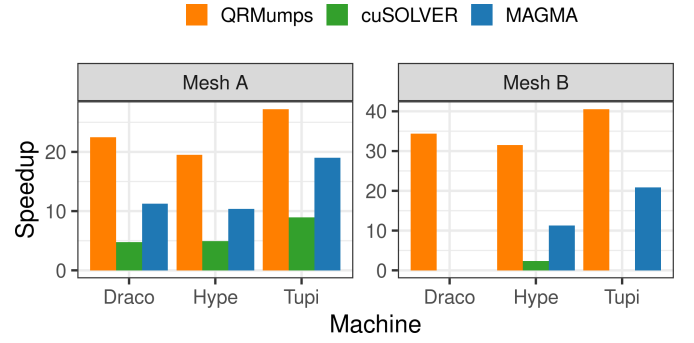


Fig. 10. Speedup values for the different machines and solvers.

as presented in Figure 8. We also point out that since we reduced the solve step time dramatically, memory copies take a significant amount of time of the iteration, as much as the entire assembly step. We can further optimize this step by using asynchronous copies and overlapping them with computation. If we manage to do this correctly, we can save up the memory copy time multiplied by the number of iterations of our application execution.

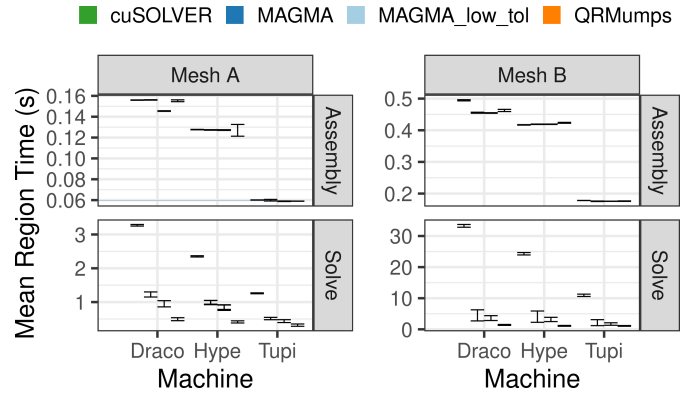


Fig. 11. Trace iteration time for different assembly and solve regions.

## VI. CONCLUSION

In this work, we presented the RAFEM application and the acceleration of its most costly phase, using parallel sparse solvers, exploring both iterative and direct solvers on multicore systems and GPU accelerators. The solvers provided speedup values ranging from 2.12 times to 40.4 times (See Figure 10 in Section V), where we noticed a lack of scalability in cuSOLVER, for which the speedup factor was lower for the bigger workload case. This scalability issue also seems to be present for this specific problem structure, where the QRMumps application presented lower speedup value for the Hype machine, which has more CPU cores than the Tupi machine, where the highest speedup value occurred. This lower value may indicate a subutilization of the computational resources, demanding an in-depth analysis to understand better what happened. We also observed the beneficial effect of newer and more powerful GPU hardware on the application acceleration. Another discussion point involves

iterative solvers tolerance, which directly affects the number of iterations needed to complete the solve step. We noticed in our experiments a reduction of the execution time when we reduced the GMRES( $m$ ) tolerance from  $10^{-10}$  to  $10^{-6}$ . However, some cases presented a minimal reduction because the RAFEM application corrector step executed more times to reach the desired convergence threshold. Thus, there is a clear trade-off between the solution numerical quality and the time needed by the iterative solver, but this also affects the number of needed corrector step iterations, where the exact relationship remains unclear for the authors. However, early experiments point out that the workload and application parameters play a role in this matter. Moreover, when using lower tolerance, the simulated values presented way more significant differences than the other solvers for mesh A as presented in IV, which can be harmful to the post-processing analysis of the results.

Lastly, future work can explore possible optimizations that can accelerate the application as the memory transfers overlap with computation and a more in-depth investigation in the QRMumps solver to help in the fine-tuning of its parameters. Finally, undoubtedly more performance can be achieved by improving the assembly stage, considering one of the many newer proposed techniques discussed in this work. The benefits of improving the assembly stage are particularly crucial for more complex geometric shapes of elements and a higher number of degrees of freedom. However, they could accelerate the RAFEM application even more. **Software and Data**

**Availability.** We endeavor to make our analysis reproducible. A public companion hosted at <https://gitlab.com/mmiletto/hpcs2020> contains the source code, datasets, and instructions to reproduce our results. A perennial archive is also available in Zenodo at <https://zenodo.org/record/4006573>.

#### ACKNOWLEDGEMENTS

We thank the following sponsors: FAPERGS MultiGPU (16/354-8) and GreenCloud (16/488-9), the CAPES/Brafitec EcoSud 182/15, the Council for Scientific and Technological Development (CNPq) under grant no 131347/2019-5 to the first author, and the CAPES/Cofecub 899/18. This study was financed in part by the Coordenação de Aperfeiçoamento de Pessoal de Nível Superior - Brasil (CAPES) - Finance Code 001. Experiments in this work used the PCAD infrastructure, <http://gppd-hpc.inf.ufrgs.br>, at INF/UFRGS.

#### REFERENCES

- [1] O. C. Zienkiewicz, R. L. Taylor, and J. Z. Zhu, *The Finite Element Method: Its Basis and Fundamentals*. Elsevier, 2005.
- [2] Y. Saad, *Iterative methods for sparse linear systems*. SIAM, 2003.
- [3] S. Tomov, R. Nath, H. Ltaief, and J. Dongarra, "Dense Linear Algebra Solvers for Multicore With GPU Accelerators," in *2010 IEEE International Symposium on Parallel Distributed Processing, Workshops and Phd Forum (IPDPSW)*, 2010, pp. 1–8.
- [4] NVIDIA, "cuSOLVER," <https://docs.nvidia.com/cuda/cusolver>, 2020.
- [5] E. Agullo, A. Buttari, A. Guermouche, and F. Lopez, "Multifrontal QR factorization for multicore architectures over runtime systems," in *European Conf. on Parallel Processing*. Springer, 2013, pp. 521–532.
- [6] P. Hénon, P. Ramet, and J. Roman, "PASTIX: a high-performance parallel direct solver for sparse symmetric positive definite systems," *Parallel Computing*, vol. 28, no. 2, pp. 301–321, 2002.
- [7] Y. Jiang, S. Mulier, W. Chong, M. C. Diel Rambo, F. Chen, G. Marchal, and Y. Ni, "Formulation of 3D finite elements for hepatic radiofrequency ablation," *International Journal of Modelling, Identification and Control*, vol. 9, no. 3, pp. 225–235, 2010.
- [8] B. M. Irons, "A frontal solution program for finite element analysis," *International Journal for Numerical Methods in Engineering*, vol. 2, no. 1, pp. 5–32, 1970.
- [9] L. Xu, K. Cai, R. Yang, Q. Lin, H. Yue, and F. Liu, "Simulation of multi-probe radiofrequency ablation guided by optical surgery navigation system under different active modes," *Computer Assisted Surgery*, vol. 21, no. 1, pp. 107–116, 2016.
- [10] D. Haemmerich and J. G. Webster, "Automatic control of finite element models for temperature-controlled radiofrequency ablation," *Biomedical engineering online*, vol. 4, no. 1, p. 42, 2005.
- [11] S. Georgescu, P. Chow, and H. Okuda, "GPU acceleration for FEM-based structural analysis," *Archives of Computational Methods in Engineering*, vol. 20, no. 2, pp. 111–121, 2013.
- [12] L. Amorim, T. Goveia, R. Mesquita, and I. Baratta, "GPU finite element method computation strategy without mesh coloring," *Journal of Microwaves, Optoelectronics and Electromagnetic Applications*, vol. 19, no. 2, pp. 252–264, 2020.
- [13] S. Sanfui and D. Sharma, "A two-kernel based strategy for performing assembly in FEA on the graphics processing unit," in *2017 International Conference on Advances in Mechanical, Industrial, Automation and Management Systems (AMIAMS)*, 2017, pp. 1–9.
- [14] U. Kiran, D. Sharma, and S. S. Gautam, "GPU-warp based finite element matrices generation and assembly using coloring method," *Journal of Computational Design and Engineering*, vol. 6, no. 4, pp. 705–718, 11 2018. [Online]. Available: <https://doi.org/10.1016/j.jcde.2018.11.001>
- [15] I. Kiss, S. Gyimothy, Z. Badics, and J. Pavo, "Parallel Realization of the Element-by-Element FEM Technique by CUDA," *IEEE Transactions on Magnetics*, vol. 48, no. 2, pp. 507–510, 2012.
- [16] J. Martínez-Frutos and D. Herrero-Pérez, "Efficient matrix-free gpu implementation of fixed grid finite element analysis," *Finite Elements in Analysis and Design*, vol. 104, pp. 61–71, 2015.
- [17] P. R. Amestoy, I. S. Duff, J.-Y. L'Excellent, and J. Koster, "MUMPS: a general purpose distributed memory sparse solver," in *International WS on Applied Parallel Computing*. Springer, 2000, pp. 121–130.
- [18] X. Yan, X. Han, D. Wu, D. Xie, B. Bai, and Z. Ren, "Research on preconditioned conjugate gradient method based on EBE-FEM and the application in electromagnetic field analysis," *IEEE Transactions on Magnetics*, vol. 53, no. 6, pp. 1–4, 2017.
- [19] J. Tu, G. H. Yeoh, and C. Liu, *Computational fluid dynamics: a practical approach*. Butterworth-Heinemann, 2018.
- [20] C. Schepke and M. Miletto, "Acceleration of Radiofrequency Ablation Process for Liver Cancer Using GPU," in *2020 28th Euromicro International Conference on Parallel, Distrib. and Network-Based Processing (PDP)*, 2020, pp. 385–389.
- [21] F. Pellegrini, "Static mapping by dual recursive bipartitioning of process architecture graphs," in *Proceedings of IEEE Scalable High Performance Computing Conference*. IEEE, 1994, pp. 486–493.
- [22] G. Karypis and V. Kumar, "A fast and high quality multilevel scheme for partitioning irregular graphs," *SIAM Journal on scientific Computing*, vol. 20, no. 1, pp. 359–392, 1998.
- [23] C. Augonnet, S. Thibault, R. Namyst, and P.-A. Wacrenier, "StarPU: a unified platform for task scheduling on heterogeneous multicore architectures," *Concurrency and Computation: Practice and Experience*, vol. 23, no. 2, pp. 187–198, 2011.
- [24] S. Thibault, "On runtime systems for task-based programming on heterogeneous platforms," HDR, Bordeaux University, 2018.
- [25] J. C. Cabral, C. E. Schaerer, and A. Bhaya, "Improving GMRES (m) using an adaptive switching controller," *Numerical Linear Algebra with Applications*, vol. 27, no. 5, p. e2305, 2020.
- [26] D. an Mey, S. Biersdorf, C. Bischof, K. Diethelm, D. Eschweiler, M. Gerndt, A. Knüpfer et al., "Score-P: A unified performance measurement system for petascale applications," in *Competence in High Performance Computing 2010*. Springer, 2011, pp. 85–97.
- [27] N. Whitehead and A. Fit-Florea, "Precision & performance: Floating point and IEEE 754 compliance for NVIDIA GPUs," *rn (A + B)*, vol. 21, no. 1, pp. 18 749–19 424, 2011.
- [28] J. Korhonen and J. You, "Peak signal-to-noise ratio revisited: Is simple beautiful?" in *Int. WS on Quality of Multimedia Exp.*, 2012, pp. 37–38.
- [29] H. Akima, A. Gebhardt, T. Petzold, and M. Maechler, "akima: Interpolation of irregularly and regularly spaced data," *R package 0.6-2*, 2016.